Proc. Natl. Acad. Sci. USA
Vol. 96, pp. 4924–4929, April 1999
Biophysics

Energy transduction in the sodium F-ATPase of *Propionigenium modestum*

PETER DIMROTH*, HONGYUN WANG†, MICHAEL GRABE‡, AND GEORGE OSTER†§

*Mikrobiologisches Institut, Eidgenössische Technische Hochschule, ETH-Zentrum, Schmelzbergstrasse 7, CH-8092 Zürich, Switzerland; and †Department of Molecular and Cellular Biology and College of Natural Resources, and ‡Department of Physics, University of California, Berkeley, CA 94720

Edited by Charles S. Peskin, New York University, New York, NY, and approved January 16, 1999 (received for review December 2, 1998)

ABSTRACT **The F-ATPase of the bacterium *Propionigenium modestum* is driven by an electrochemical sodium gradient between the cell interior and its environment. Here we present a mechanochemical model for the transduction of transmembrane sodium-motive force into rotary torque. The same mechanism is likely to operate in other F-ATPases, including the proton-driven F-ATPases of *Escherichia coli*.**

The culmination of metabolism is the generation of ATP from a transmembrane electromotive gradient. This conversion of electrochemical energy into the chemical energy of the terminal phosphoric anhydride bond of ATP is accomplished by the enzyme ATP synthase—also called F_1F_o-ATP synthase, or F_1F_o-ATPase. The latter name reflects the fact that the enzyme is reversible and can act as a proton (or Na^+) -pumping ATPase. Closely related ATP synthases are found in the bacterial cytoplasmic membrane, the inner membrane of mitochondria, and the thylakoid membrane of chloroplasts. These enzymes consist of a membrane-embedded portion, F_o, which contains the ion channel, and the soluble F_1 moiety, which harbors the nucleotide-binding sites in which ATP is synthesized or hydrolyzed (for reviews see refs. 1–6).

Fig. 1 shows a schematic diagram of ATP synthase that summarizes a great deal of experimental work. Isolated F_1 (also called F_1-ATPase) hydrolyzes ATP and is composed of subunits $\alpha_3\beta_3\gamma\delta\varepsilon$ (subscripts refer to the subunit stoichiometry). The majority of the $\alpha_3\beta_3\gamma$ structure has been solved by x-ray crystallography (7). The structure shows a cylinder formed by the three α and three β subunits alternating around a central cavity through which the asymmetrically bent shaft of the γ subunit extends and protrudes. The γ subunit asymmetry correlates with the different conformations assumed by each of the three catalytic βs, in accordance to Boyer's "binding change mechanism" (8). This strongly supports the view that the binding changes of the β subunits are coupled to the rotation of the γ subunit. This rotational coupling is confirmed by several recent studies which demonstrate unequivocally that ATP hydrolysis drives rotation of the γ subunit within the $\alpha_3\beta_3\gamma$ subcomplex of F_1 (9–12), and that subunit ε rotates with γ as a unit (13, 14). The rotation is reversed during ATP synthesis, driven by the downhill movement of the coupling ions through the F_o sector.

The F_o portion of ATP synthase has been most intensely studied with the enzymes from the bacteria *Escherichia coli* and *Propionigenium modestum*. The subunit composition of F_o is ab_2c_{12}. The c subunit consists of twin membrane-spanning α-helices that are connected by a cytoplasmic loop. Evidence from electron and atomic force microscopy indicates that the c subunits are assembled into a 12-unit ring that is flanked at the periphery by the a and the two b subunits (15–17). The b subunits attach the a subunit to an α subunit of the $\alpha_3\beta_3$ headpiece via the δ subunit (18, 19). The a subunit is an integral membrane protein consisting of five or six membrane-spanning α-helices (20–23). According to NMR analyses of *E. coli* subunit c in chloroform/methanol/water, the two helices pack closely to one another, extending over 40 and 30 residues, respectively, with a short interruption after D61 of the C-terminal α-helix (24). The proton-binding D61 residue was postulated to reside within the middle of the membrane. Recent NMR structure analyses of *P. modestum* subunit c in dodecyl sulfate micelles revealed folding into four clearly defined α-helices of which the N- and C-terminal helices are the most hydrophobic and of sufficient length to span the membrane (U. Matthey, G. Kaim, P.D., D. Braun, and K. Wüthrich, unpublished results). The α-helical structure is interrupted on both strands in the Na^+-binding site region (Q32, E65, S66) (25). This observation suggests that the site is located at the cytoplasmic boundary of the membrane and that the additional two helices and the loop are cytoplasmic or membrane-associated but not membrane-integral. This location of the binding site is consistent with biochemical evidence showing that the binding sites of more than one c subunit are readily accessible from the aqueous phase (26).

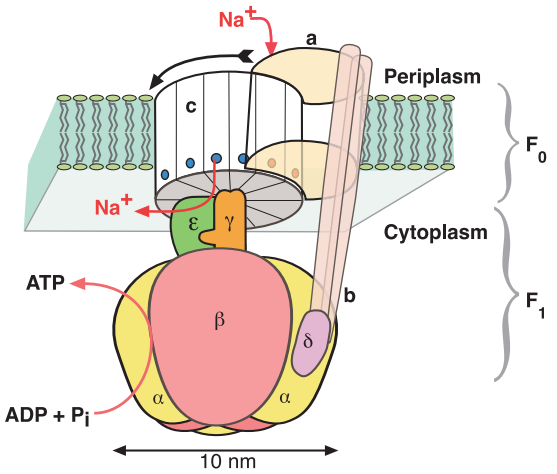

FIG. 1. Schematic diagram of the Na^+ F_oF_1 ATPase. The rotor consists of subunits $c_{12}\gamma\varepsilon$, and the stator consists of subunits $ab_2\delta(\alpha\beta)_3$. Six nucleotide-binding sites lie at the $\alpha\beta$ interfaces; three catalytic sites alternate with three noncatalytic sites. The arrow indicates the direction of rotation during ATP synthesis.

The overall construction of the F_o and F_1 sectors has the structure of a counter-rotating "rotor" and "stator" assembly comprising, respectively, $c_{12}\gamma\varepsilon$ and $ab_2\delta\alpha_3\beta_3$. Indeed, several lines of evidence with the ATP synthase of *P. modestum* strongly supports the idea that the c and a subunit assemblies counter-rotate during the translocation of the coupling Na^+

The publication costs of this article were defrayed in part by page charge payment. This article must therefore be hereby marked "*advertisement*" in accordance with 18 U.S.C. §1734 solely to indicate this fact.

PNAS is available online at www.pnas.org.

This paper was submitted directly (Track II) to the *Proceedings* office. A Commentary on this article begins on page 4735.

§To whom reprint requests should be addressed. e-mail: goster@nature.berkeley.edu.

ions: (*i*) Mutants within subunits c or a that alter the coupling ion specificity were isolated, showing a specific interaction of either subunit with the coupling ions (25, 27, 28). (*ii*) In an ATPase with a Na^+-impermeable a subunit mutation, 1 Na^+ per ATPase was occluded in an ATP-dependent fashion (26). (*iii*) In the mutant enzyme with partially dicyclohexyl carbodiimide-modified c subunits, Na^+ occlusion was impaired when ATP was added first and Na^+ second, but not when this order was reversed (29). (*iv*) With the wild-type enzyme reconstituted into proteoliposomes, Na^+ ions were rapidly exchanged between the two compartments of the membrane. The exchange was abolished when the system switched from an idling into a torque-generating operation mode, either by the hydrolysis of ATP or with the driving force provided by an electric potential (29). Interestingly, a Na^+ concentration gradient was unable to induce the switch; ATP synthesis by the enzymes from *P. modestum* or *E. coli* depended on the electric potential (29, 30).

On the basis of these and other data, several authors have proposed qualitative models for how ion flow generates counter-rotation of the rotor and stator segments of ATP synthase (9, 26, 29, 31–33). Of these, only Elston, *et al.* (33) provided a quantitative account of how a rotary torque is generated by the transmembrane electrochemical gradient (33). In their model, they did not take into account the role of the membrane potential or the property elaborated for *P. modestum* that the rotor ion-binding sites (E65) are in equilibrium with the cytoplasm. With this picture of the *P. modestum* motor in mind, we have constructed a model that incorporates this new information and can account quantitatively for most of the experimental data on the *P. modestum* F_o motor.

A Quantitative Model for the F_o Motor of *P. modestum*

During ATP synthesis, the rotor turns clockwise as viewed from the periplasm. This unidirectional rotation requires an asymmetry somewhere in the rotor–stator assembly. The rotor, consisting of 12 double α-helices, is thought to form a symmetrical disk into which the γ-shaft inserts (34). If so, the asymmetry must exist on the stator—in particular, on the a subunit because that is the only stator element that abuts the rotor. Fig. 2*a* shows a schematic view of the rotor–stator model we are proposing here. The rotor–stator interface must present a hydrophobic barrier against leakage of ions from the periplasm to the cytoplasm. Thus the ion channel should not provide an uninterrupted path connecting the periplasm with the cytoplasm. The fundamental asymmetry that determines the direction of rotation in our model is the horizontal hydrophilic strip at the rotor–stator interface that connects the half-channel laterally to the cytoplasm; this is shown face-on in Fig. 2*b*. This hydrophilic strip permits charged (unoccupied) rotor sites to enter the rotor–stator interface from the right and pass as far to the left as the edge of the stator channel. We place the positive stator charge (R227) close to the strip. This positioning has the dual effect of repelling ions in the channel—thus preventing ion leakage—and attracting unoccupied negative rotor sites when they enter the rotor–stator interface. Entering rotor sites are very likely to be empty for two reasons. First, the rotor sites are in equilibrium with the cytoplasmic reservoir; therefore, because the cytoplasmic ion concentration is low, the sites will be mostly unoccupied. Second, an occupied rotor site that enters the rotor–stator interface and approaches the stator charge will have its pK_a (i.e., binding affinity) reduced, causing it to give up its sodium ion to the cytoplasmic reservoir.

A negatively charged (unoccupied) rotor site residing in the channel interacts electrostatically with the stator in another important way. A charged site attempting to leave the channel (to the left in Fig. 2) and enter the hydrophobic rotor–stator

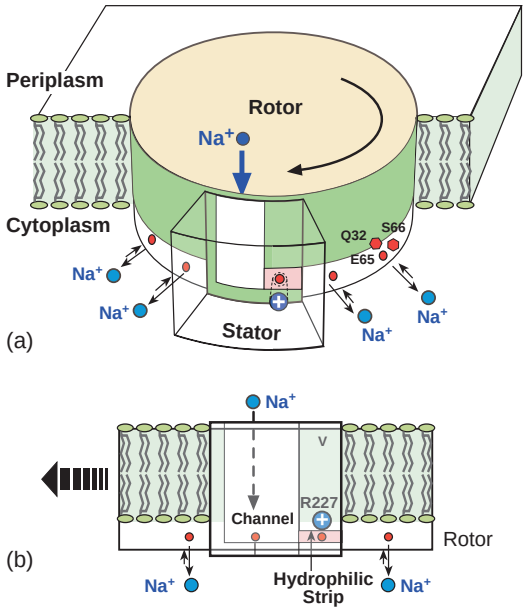

FIG. 2. (*a*) Schematic of the rotor–stator assembly in *P. modestum*. During ATP synthesis, the rotor turns to the left (clockwise viewed from the periplasm). The rotor section below the level of the membrane contains the 12 ion-binding sites. Each site consists of the triad Q32/E65/S66, which coordinates a sodium ion. The stator contains an aqueous channel that conducts ions from the periplasmic (positive) reservoir to the level of the horizontal hydrophilic strip. The positive stator charge, R227, blocks leakage of ions along this strip to the cytoplasm. (*b*) Face-on view of the rotor–stator assembly. Rotation during synthesis is to the left. There are four rotor sites located near the stator, two within the rotor–stator interface and two adjacent laterally. The stator is penetrated by an aqueous channel that admits ions from the periplasm, but ions can exit to the cytoplasm only by boarding a rotor site and passing through the dielectric barrier forming the left wall of the channel. If the occupied site moves to the right, it quickly loses its ion back to the channel when it approaches the positive stator charge, R227.

interface encounters an electrostatic barrier arising from the discontinuity in the dielectric constant between the aqueous channel, ε_c, and the stator, ε_s (see the discussion below). To pass through the stator to the left the rotor site must bind an ion from the channel. When occupied by a sodium ion the electrostatic field of the site is reduced to a dipole, and it can be considered almost neutral. Thus occupied, a site faces but a small electrostatic barrier when leaving the channel to the left. The stator charge ensures that an occupied site moving to the right will quickly lose its ion back to the channel. To deduce the consequences of these rotor–stator interactions we must formulate them quantitatively as follows.

The rotor sites outside the stator are in contact with the cytoplasm, and the site in the stator channel is in contact with the periplasm. However, the rotor–stator interaction depends only on the ionization state of the 4 rotor sites within and adjacent to the stator. Thus the chemical state of the rotor–stator assembly, denoted by **s,** has $2^4 = 16$ possibilities because each of these 4 sites may be occupied or empty. Transitions between states occur when a site binds or releases a sodium ion. Because the relaxation to equilibrium after a proton association/dissociation event is much faster than the mechanical motion of the rotor, we can treat the transitions between these states as a Markov chain (33). Because of the electrostatic interactions between the rotor sites and the stator charge, the transitions between states depend on the angular position of the rotor, denoted θ. The evolution of the rotor's chemical state is symbolically described by the equation (see the supplemental data on the PNAS web site, www.pnas.org):

$$\frac{d\mathbf{s}}{dt} = \mathbf{K}(\theta)\mathbf{s}, \qquad [1]$$

where $\mathbf{K}(\theta)$ is the matrix of transition rates between the chemical states. The motion of the rotor can be described by equating the viscous drag on the rotor to the torques that act on the rotor and the Brownian force modeling the rotor's thermal fluctuations [i.e., the Langevin equation (35, 36)]:

$$\underbrace{\zeta \frac{d\theta}{dt}}_{\text{Frictional drag}} = \underbrace{\tau_Q(\theta, \mathbf{s})}_{\text{Rotor–stator charge interaction}} + \underbrace{\tau_{\Delta\psi}(\theta, \mathbf{s})}_{\text{Membrane potential}} + \underbrace{\tau_{\Delta\varepsilon}(\theta, \mathbf{s})}_{\text{Dielectric barrier}} + \underbrace{\tau_{RS}(\theta)}_{\text{Rotor–stator passive interaction}} - \underbrace{\tau_L(\theta)}_{\text{Load torque from } F_1} + \underbrace{\tau_B(t)}_{\text{Brownian torque}},$$

$$\underbrace{\mathbf{s} = 1, \ldots, 16}_{\text{Chemical states}} \qquad [2]$$

The terms on the right-hand side of Eq. **2** are as follows (the computations are detailed in the supplemental data published on the PNAS web site, www.pnas.org).

(*i*) $\tau_Q(\theta, \mathbf{s})$ is due to the electrostatic interaction between the stator charge (R227) and the rotor sites that are within the hydrophilic rotor–stator strip. The charged (unoccupied) site will be attracted by the stator charge (R227) according to Coulomb's law corresponding to the dielectric and shielding environment of the stator.

(*ii*) $\tau_{\Delta\psi}(\theta, \mathbf{s})$ is due to the membrane potential drop across the horizontal segment between the periplasmic channel and the stator boundary.

(*iii*) $\tau_{\Delta\varepsilon}(\theta, \mathbf{s})$ is the electrostatic barrier that opposes the entry of a charged site into the hydrophobic rotor–stator interface.¶

(*iv*) $\tau_{RS}(\theta)$ is the passive rotor–stator interaction. We will discuss the origin and role of this term in *Results*.

(*v*) $\tau_L(\theta)$ is the load exerted by F_1 on the rotor through the γ-shaft.

(*vi*) $\tau_B(t)$ is the random Brownian torque due to the thermal fluctuations of the rotor.

As indicated by their dependence on **s**, the three electrostatic torques depend on the chemical state of the rotor site; that is, whether a site is charged (unoccupied) or uncharged (occupied).

In summary, the following effects combine to drive the rotor.

(*i*) The stator charge (R227) attracts an unoccupied rotor site; blocks leaking of ions through the channel; and lowers the binding affinity (pK_a) of rotor sites, causing the mobile ion to dissociate as an occupied rotor site approaches it.

The last two effects couple the rotation of the motor tightly to the ion flux through the rotor–stator interface.

(*ii*) The membrane potential creates an electrostatic gradient that biases the thermal escape of the rotor site from the positive stator charge (R227) into the periplasmic channel (to the left in Fig. 2); and decreases the dissociation rate of sodium ions from the rotor site to the periplasmic reservoir.

The extent of these two effects depends on the fraction of the total voltage drop across the horizontal segment and the periplasmic channel. We shall assume that the channel is aqueous and that most of the voltage drop is across the horizontal segment.

¶The height of this barrier is given approximately by $\approx 200\ [(1/\varepsilon_c) - (1/\varepsilon_s)] \approx 45 k_B T \approx 27$ kcal/mol (k_B is the Boltzmann constant and T is the absolute temperature; 1 kcal = 4.18 J), where ε_c and ε_s are the dielectric constants of the aqueous channel and the stator, respectively (37).

(*iii*) The dielectric barrier at the left of the channel prevents an unoccupied rotor site from entering the stator from the left in Fig. 2.

(*iv*) Brownian motion drives rotational diffusion of the rotor.

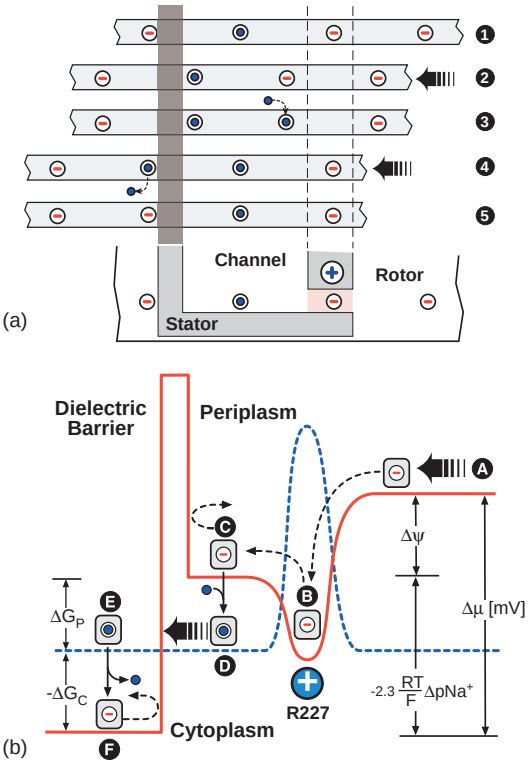

FIG. 3. (*a*) A typical sequence of events that advance the rotor by one step of $2\pi/12$. Consider the initial position of the rotor shown at ❶. The third site from the left is held in the electrostatic well of the stator charge. Step ❶ → ❷: the rotor fluctuates until the third (empty) site thermally jumps out of the potential well of the stator charge. This jump is biased by the transmembrane potential and is helped by the dielectric barrier preventing the first (empty) rotor site from entering the low-dielectric medium of the stator from the right. ❷ → ❸: once the third rotor site is out of the potential well of the stator charge, it quickly binds a sodium ion from the periplasmic (acidic) reservoir. ❸ → ❹: the positive stator charge pulls the empty fourth rotor site into its potential well. Because the second rotor site is neutralized, it can pass through the dielectric barrier. ❹ → ❺: once the second rotor site passes out of the stator its sodium ion quickly dissociates into the cytoplasmic reservoir. Once empty, it cannot go back into the low dielectric rotor–stator interface. ❺ is exactly the same state as ❶, but shifted to the left by one rotor step. (*b*) Free energy diagram of one rotor site as it passes through the rotor–stator interface. The chemical reactions of ion binding and dissociation to the rotor site switch the potentials seen by the rotor site between that corresponding to an empty site (solid line) and that corresponding to a neutralized site with an ion bound (broken line). Step **A** → **B**: the rotor diffuses to the left, bringing the empty (negatively charged) site into the attractive field of the positive stator charge (R227). **B** → **C**: once the site is captured, the membrane potential biases the thermal escape of the site to the left (by tilting the potential and lowering the left edge). **C** → **D**: the site quickly picks up an ion from the periplasmic channel, which drops the site to the neutralized site potential (broken line). **D** → **E:** this allows the occupied site to pass through the dielectric barrier. (If the site diffuses to the right, the ion quickly dissociates from the site as it approaches the stator charge.) **E** → **F**: upon exiting the stator the site loses its sodium ion. Now charged, the site sees the stator dielectric barrier, which prevents back-diffusion. The cycle decreases the free energy of the system by an amount equal to the electromotive force: $\Delta\mu = \Delta\psi - 2.3(RT/F)\Delta pNa$, where R is the gas constant, F is the Faraday constant, and pNa is the negative log of the Na concentration. The free energy changes accompanying ion binding from the periplasm (P) and dissociation to the cytoplasm (C) are $\Delta G_P = -(2.3RT/F)(pK_a - pNa_P)$ and $\Delta G_C = -(2.3RT/F)(pNa_C - pK_a)$, respectively.

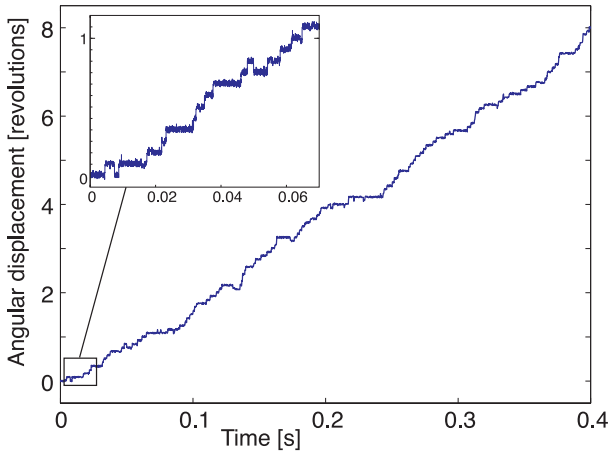

FIG. 4. Trajectory of the rotor position, $\theta(t)$. The motor advances stochastically in steps of $2\pi/12$, with a mean velocity (slope) of ≈20 Hz. There are occasional reversals whose frequency increases with the Na^+ concentration in the cytoplasm because the dielectric barrier is seen only by empty sites.

Eqs. **1** and **2** describe how these effects combine to drive the rotor. Solutions of the model equations will be presented below; however, an intuitive picture of how the motor works is shown in Fig. 3*a*, which depicts one sequence of events that advance the rotor by 1 rotor unit, $2\pi/12$. The mechanism of energy transduction is summarized in Fig. 3*b*, which shows a projection of the free energy onto a rotor site as the site moves through the stator. The binding and dissociation of ions to the rotor site switches the electrostatic potential seen by the rotor, which biases the rotor's diffusion to the left.

To summarize: The sodium motor is driven by biased diffusion of the rotor, the bias provided by the three electrostatic effects listed above. Note that the membrane potential can be viewed as a "power stroke"; however, in the absence of rotor diffusion it cannot drive the motor to the left. Rather, it biases the thermal escape of the rotor to the left.

RESULTS

The Motor Advances Stepwise with Occasional Reversals. The first requirement of the model is that it rotate at the correct rate and be capable of generating the torque required to release ATP from the catalytic sites of F_1 (8). Fig. 4 shows a trajectory of the motor when subject to a load of 45 pN·nm. The motor advances stochastically in steps of $2\pi/12$ at a rate of 20 Hz, with occasional reversals. This rotation rate corresponds to an ATP synthesis rate of ≈60 per s (3 ATP per revolution of γ, corresponding to an average of 4 Na^+/ATP). This is consistent with the estimated synthesis rate of *E. coli* and *P. modestum* (P.D., unpublished results).

The Motor Generates a Torque Sufficient to Produce ATP. In Fig. 5 we have plotted the rotation rate as a function of the resisting load from F_1 [$\tau_L(\theta)$ in Eq. **2**] for two extreme situations: (*i*) when the torque is generated completely by the membrane potential, $\Delta\psi$ (solid line), and (*ii*) when it is generated completely by the ion concentration difference (broken line); combinations lie between the two curves. The figure shows that the model can reproduce the observed synthesis rate when subjected to the required load. When the passive interaction between the rotor and stator is negligible, Fig. 5*a* shows that the membrane potential and the concentration difference contribute about equally to torque generation. For a load torque between 40 and ≈50 pN·nm, the rotation rate is 100 to ≈150 Hz, which corresponds to a synthesis rate of ≈400 per s.

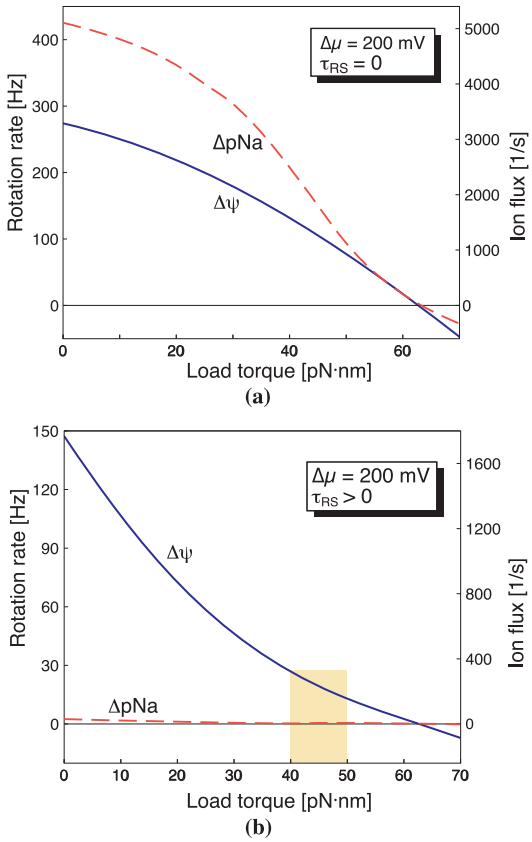

FIG. 5. The motor rotation rate and sodium flux as functions of the load torque. Lines represent the velocity; the sodium flux is tightly coupled and so the flux curves are superimposed on the rotation curves. Each panel compares the results for two different forms of the sodium motive force. Solid lines, the motor is completely driven by the membrane potential, $[Na^+]_P = [Na^+]_C = 1$ mM and $\Delta\psi = 200$ mV. Broken lines, the motor is completely driven by the ion concentration difference, $[Na^+]_P = 300$ mM, $[Na^+]_C = 0.1$ mM, and $\Delta\psi = 0$. (*a*) Load–velocity curve when the passive rotor–stator interaction, τ_{RS}, = 0. In this case, the membrane potential and concentration difference contribute about equally to the torque. (*b*) Load–velocity curve when the passive rotor–stator interaction, τ_{RS}, ≠ 0. In this case, the rate-limiting step is the rotor diffusing out of the retarding potential between the rotor and stator, and the torque is generated almost completely by the membrane potential.

The situation appears to be quite different for bacteria. The ATP synthases of *P. modestum* and *E. coli* produce ATP at a much lower rate, ≈50 molecules per s; that is, at physiological operating conditions, the rotation rate is 15–20 Hz. To reduce the model's rotation rate sufficiently we had to slow the motor by introducing an additional retarding interaction (electrostatic, steric, or both) between the rotor and the stator (τ_{RS} in Eq. **2**). Since the rotor is $2\pi/12$ symmetrical, we modeled the interaction, $\tau_{RS}(\theta)$, by a $2\pi/12$ periodic potential with a depth of ≈10 k_BT; the shape of this potential proved irrelevant. This slowed the rotation rate to the physiological range of *P. modestum*, as shown in Fig. 5*b*. The concomitant result of adding this interaction is that the rotation is driven almost completely by the membrane potential, with the concentration difference playing almost no role in torque generation. Indeed, this is just the situation observed under experimental conditions (29, 30).

The Idle Motor Catalyzes the Exchange of Sodium Ions. An important check on the assumptions of the model can be obtained from the sodium exchange experiments of Kaim *et al.* (29). In these experiments, liposomes with ATPase of *P. modestum* incorporated contained 100 mM NaCl. When the liposomes were exposed to a bath of radioactively labeled 2

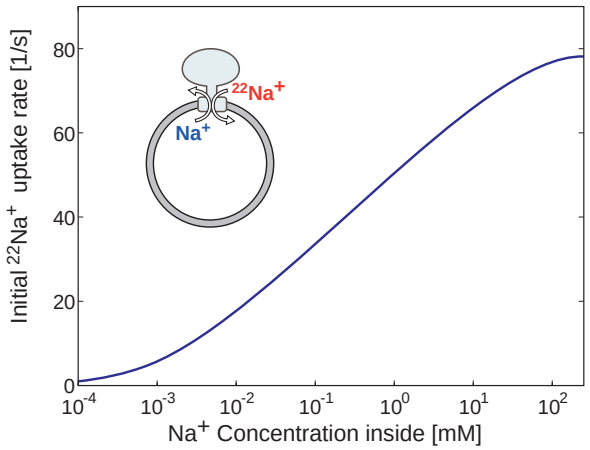

FIG. 6. Sodium exchange experiment (see text). The computation is explained in the supplemental data published on the PNAS web site (www.pnas.org).

mM ^{22}NaCl outside, sodium ions exchanged between the inside and outside, causing a flow of $^{22}Na^+$ from outside to inside against a 50-fold concentration gradient.

With no potential difference between the inside and outside of the liposomes, the sodium concentration gradient cannot overcome the free energy barrier of the rotor and stator interaction, and the motor will not rotate. However, the rotor can fluctuate and carry a rotor site back and forth through the low-dielectric region of the stator separating the outside and the inside of the liposomes. Because a rotor site must be occupied to pass through this low-dielectric region, each time the rotor site cycles through the region and back, it carries one sodium ion from outside to inside and one from inside to outside. Fig. 6 shows the initial $^{22}Na^+$ uptake rate as a function of the Na^+ concentration inside the liposomes. The $^{22}Na^+$ uptake decreases as the Na^+ concentration inside the liposomes is reduced. This result is consistent with the observation of Kaim and Dimroth (29) that $^{22}Na^+$ uptake stops if concentration inside is zero.

The Motor Operates in Reverse as an Ion Pump. Finally, we require that the motor be capable of performing as an ion pump when driven in reverse by a torque generated in F_1 from ATP hydrolysis. We have plotted in Fig. 7 the ion pumping behavior against a range of membrane potentials. In this calculation the motor is driven in reverse by the torque generated in F_1 corresponding to an ATP concentration of 1 mM (38).

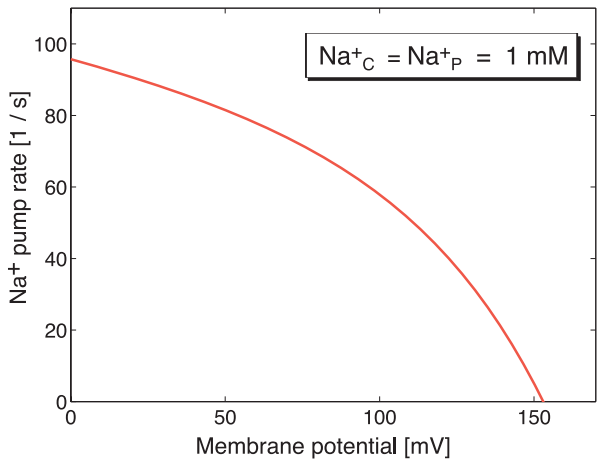

FIG. 7. The sodium pump rate is plotted versus membrane potential when the F_o motor is driven backwards as a pump by the F_1 motor hydrolyzing ATP. The computation is explained in the supplemental data published on the PNAS web site (www.pnas.org).

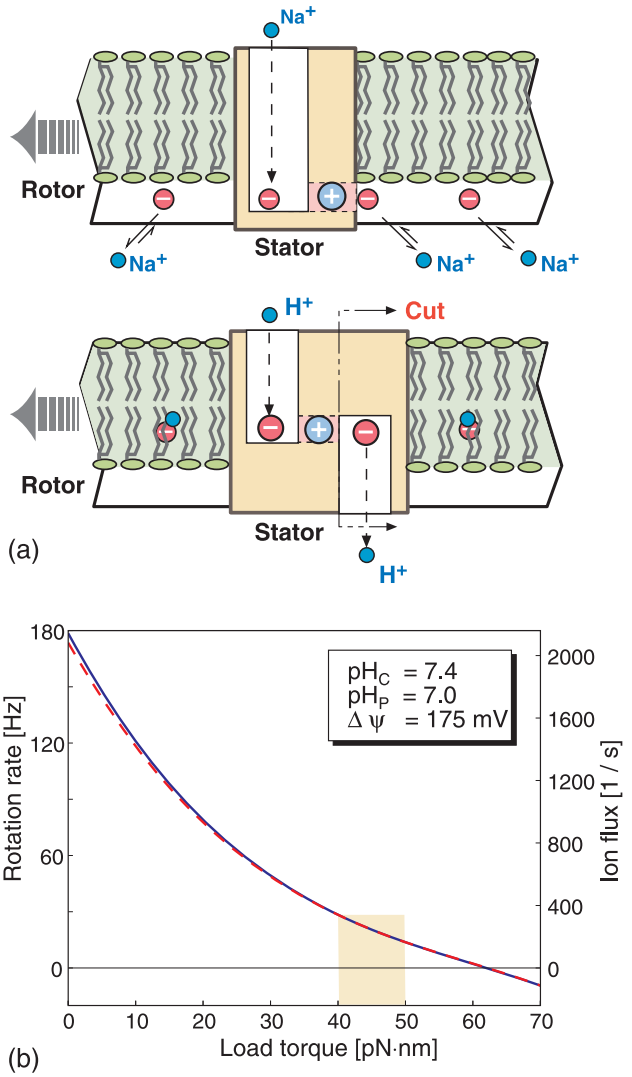

FIG. 8. (*a*) The relationship between the one-channel model of *P. modestum* (*Upper*) and the two-channel model of *E. coli* (*Lower*) (33). In *E. coli* the rotor sites (D61) may not be accessible from the cytoplasm, but only via a cytoplasmic half-channel. In the sodium motor the cytoplasmic channel is unnecessary because the rotor sites (E65) are accessible directly to the cytoplasmic reservoir. The *E. coli* stator can be converted to the *P. modestum* stator simply by cutting off the cytoplasmic channel and moving the row of rotor sites below the membrane level. (*b*) Comparison of the load–velocity curves for the one-channel model (solid line) and the two-channel model (broken line) applied to the proton-driven *E. coli* motor. The two models perform practically the same.

The Same Operating Principle Can Drive the Proton F-ATPases. In the proton F_o ATPases, there is some evidence that the rotor site (D61 in *E. coli*) is not accessible from the cytoplasm as it is in the sodium motor (22, 24, 39). To deal with this situation, Elston *et al.* (33) proposed a model for torque generation in the proton F_o motor of mitochondria and *E. coli*. Fig. 8*a* shows the structural comparison between the one-channel model described above and the two-channel model in ref. 33. The principle of operation is the same in both variants: electrostatic forces bias the rotational diffusion of the rotor. However, Elston *et al.* assumed that the membrane potential drop takes place entirely across the half-channels, so it plays no role in biasing the escape of a rotor site from the grasp of the stator charge. Fig. 8*b* shows a comparison between the load–velocity behavior of the two models when the same potential drop exists across the horizontal hydrophilic strip. The parameter

Table 1. Parameter values used in the simulations

Parameter	H^+ ATPase	Na^+ ATPase
Ion diffusion constant (D_I), $nm^2 \cdot s^{-1}$	9.3×10^9	1.0×10^9
Diffusion constant of rotor (D_r), s^{-1}	1.0×10^4	1.0×10^4
Dielectric constant of stator (ε_s)	4.0	4.0
Bilayer viscosity (η), poise	10	10
Radius of rotor (R), nm	3	3
Ion conductivity of channel, $M^{-1} \cdot s^{-1}$	1.2×10^{11}	1.2×10^7
pK_a of rotor sites	7.1	3.5
Concentration of periplasmic side	$pH_P = 7.0$	$[Na^+]_P = 1.0$ mM
Concentration of cytoplasmic side	$pH_C = 7.4$	$[Na^+]_C = 1.0$ mM
Membrane potential ($\Delta\psi$)	175 mV = 7 k_BT	200 mV = 8.0 k_BT

values used in the computations are listed in Table 1. We see that the two perform nearly identically.

CONCLUSIONS

We have presented a model for the mechanochemistry of the sodium F_o-ATPase of *P. modestum* that is in quantitative agreement with the chemical, mechanical, and structural experimental data. The motor is driven by a combination of electrostatic effects: Negatively charged rotor sites that diffuse into the rotor–stator interface are captured by the positive stator charge, R227. Thermal fluctuations permit the captured site to escape long enough to pick up an ion from the periplasmic channel. This escape is biased by the membrane potential. When occupied, a rotor site is nearly neutral, and it can then pass through the hydrophobic rotor–stator interface to the cytoplasm. Once a site has lost its ion to the cytoplasm its diffusive motions are ''ratcheted'': it cannot move backwards into the hydrophobic portion of the rotor–stator interface. Thus the rotor progresses driven by a combination of electrostatic attraction and biased diffusion (40). This mechanism is capable of generating sufficient torque to release ATP from the catalytic sites of F_1 in accordance with the binding change mechanism. When driven in reverse, the motor performs as an efficient sodium pump, which suggests a relationship with the structurally similar V-ATPase proton pumps—a connection that will be treated in a subsequent publication. Finally, we should note that there are similarities between the model presented here and the model of Berg and Kahn for the bacterial flagellar motor (41, 42). This similarity is perhaps not surprising because it has long been speculated that there is an evolutionary relationship between the two. This also suggests that the mechanism elucidated here may be employed widely by cells to convert transmembrane electrochemical gradients into mechanical motions.

G.O. and H.W. were supported by National Science Foundation Grant DMS 9220719.

1. Futai, M., Omote, H. & Maeda, M. (1995) *Biochem. Soc. Trans.* **23,** 785–789.
2. Fillingame, R. (1990) in *Molecular Mechanics of ATP Synthesis by F_1F_o-Type Proton-Transporting ATP Synthases*, Bacterial Energetics, ed. Krulwich, T. (Academic, London), Vol. 12, pp. 345–392.
3. Deckers-Hebestreit, G. & Altendorf, K. (1996) *Annu. Rev. Microbiol.* **50,** 791–824.
4. Dimroth, P. (1997) *Biochim. Biophys. Acta* **1318,** 11–51.
5. Weber, J. & Senior, A. E. (1997) *Biochim. Biophys. Acta* **1319,** 19–58.
6. Allison, W. (1998) *Acc. Chem. Res.* **31,** 819–826.
7. Abrahams, J., Leslie, A., Lutter, R. & Walker, J. (1994) *Nature (London)* **370,** 621–628.
8. Boyer, P. (1993) *Biochim. Biophys. Acta* **1140,** 215–250.
9. Duncan, T. M., Bulygin, V. V., Zhou, Y., Hutcheon, M. L. & Cross, R. L. (1995) *Proc. Natl. Acad. Sci. USA* **92,** 10964–10968.
10. Sabbert, D., Engelbrecht, S. & Junge, W. (1996) *Nature (London)* **381,** 623–625.
11. Noji, H., Yasuda, R., Yoshida, M. & Kinosita, K. (1997) *Nature (London)* **386,** 299–302.
12. Yasuda, R., Noji, H., Kinosita, K. & Yoshida, M. (1998) *Cell* **93,** 1117–1124.
13. Capaldi, R., Aggeler, R., Wilkens, S. & Gruber, G. (1996) *J. Bioenerg. Biomembr.* **28,** 397–401.
14. Kato-Yamada, Y., Noji, H., Yasuda, R., Kinosita, K., Jr., & Yoshida, M. (1998) *J. Biol. Chem.* **273,** 19375–19377.
15. Birkenhager, R., Hoppert, M., Deckers-Hebestreit, G., Mayer, F. & Altendorf, K. (1995) *Eur. J. Biochem.* **230,** 58–67.
16. Singh, S., Turina, P., Bustamante, C. J., Keller, D. J. & Capaldi, R. (1996) *FEBS Lett.* **397,** 30–34.
17. Takeyasu, K., Omote, H., Nettikadan, S., Tokumasu, F., Iwamoto-Kihara, A. & Futai, M. (1996) *FEBS Lett.* **392,** 110–113.
18. Lill, H., Hensel, F., Junge, W. & Engelbrecht, S. (1996) *J. Biol. Chem.* **271,** 32737–32742.
19. Ogilvie, I., Aggeler, R. & Capaldi, R. A. (1997) *J. Biol. Chem.* **272,** 16652–16656.
20. Yamada, H., Moriyama, Y., Maeda, M. & Futai, M. (1996) *FEBS Lett.* **390,** 34–38.
21. Jäger, H., Birkenhäger, R., Stalz, W. D., Altendorf, K. & Deckers-Hebestreit, G. (1998) *Eur. J. Biochem.* **251,** 122–132.
22. Long, J. C., Wang, S. & Vik, S. B. (1998) *J. Biol. Chem.* **273,** 16235–16240.
23. Valiyaveetil, F. & Fillingame, R. (1998) *J. Biol. Chem.* **273,** 16241–16247.
24. Girvin, M., Rastogi, V., Abildgaard, F., Markley, J. & Fillingame, E. (1998) *Biochemistry* **37,** 8817–8824.
25. Kaim, G., Wehrle, F., Gerike, U. & Dimroth, P. (1997) *Biochemistry* **36,** 9185–9194.
26. Kaim, G., Matthey, U. & Dimroth, P. (1998) *EMBO J.* **17,** 688–695.
27. Kaim, G. & Dimroth, P. (1995) *J. Mol. Biol.* **253,** 726–738.
28. Kaim, G. & Dimroth, P. (1998) *Biochemistry* **37,** 4626–4634.
29. Kaim, G. & Dimroth, P. (1998) *EMBO J.* **17,** 5887–5895.
30. Kaim, G. & Dimroth, P. (1998) *FEBS Lett.* **434,** 57–60.
31. Junge, W., Lill, H. & Engelbrecht, S. (1997) *Trends Biochem. Sci.* **22,** 420–423.
32. Vik, S. B. & Antonio, B. J. (1994) *J. Biol. Chem.* **269,** 30364–30369.
33. Elston, T., Wang, H. & Oster, G. (1998) *Nature (London)* **391,** 510–514.
34. Groth, G. & Walker, J. (1997) *FEBS Lett.* **410,** 117–123.
35. Gardiner, C. (1985) *Handbook of Stochastic Methods* (Springer, New York).
36. Risken, H. (1989) *The Fokker-Planck Equation* (Springer, New York).
37. Israelachvili, J. (1992) *Intermolecular and Surface Forces* (Academic, New York).
38. Wang, H. & Oster, G. (1998) *Nature (London)* **396,** 279–282.
39. Jones, P., Jiang, W. & Fillingame, R. (1998) *J. Biol. Chem.* **273,** 17178–17185.
40. Peskin, C. S., Odell, G. M. & Oster, G. (1993) *Biophys. J.* **65,** 316–324.
41. Berg, H. & Khan, S. (1983) in *A Model for the Flagellar Rotary Motor*, eds. Sund, H. & Veeger, C. (de Gruyter, Berlin), pp. 485–497.
42. Meister, M., Caplan, S. R. & Berg, H. C. (1989) *Biophys. J.* **55,** 905–914.

Supplementary Material

Here we supply some additional material justifying the model construction and details on how the numerical computations were carried out.

Topology of the a Subunit and the Rotor-Stator Assembly

Fig. 9 shows the topology and amino acid sequence of the a-subunit from *P. modestum*. Considering the α-helical packing, it is likely that the rotor-stator interface consists of at least three stator helices; the pattern of charged and polar residues is consistent with the putative structure shown in Fig. 10. The rotor-stator interface must present a hydrophobic barrier against leakage of ions from the periplasm to the cytoplasm; thus the ion channel should not penetrate all the way through the stator, so that there is no direct path connecting the periplasm with the cytoplasm. To accommodate these constraints we propose the rotor-stator model shown in Fig. 11.

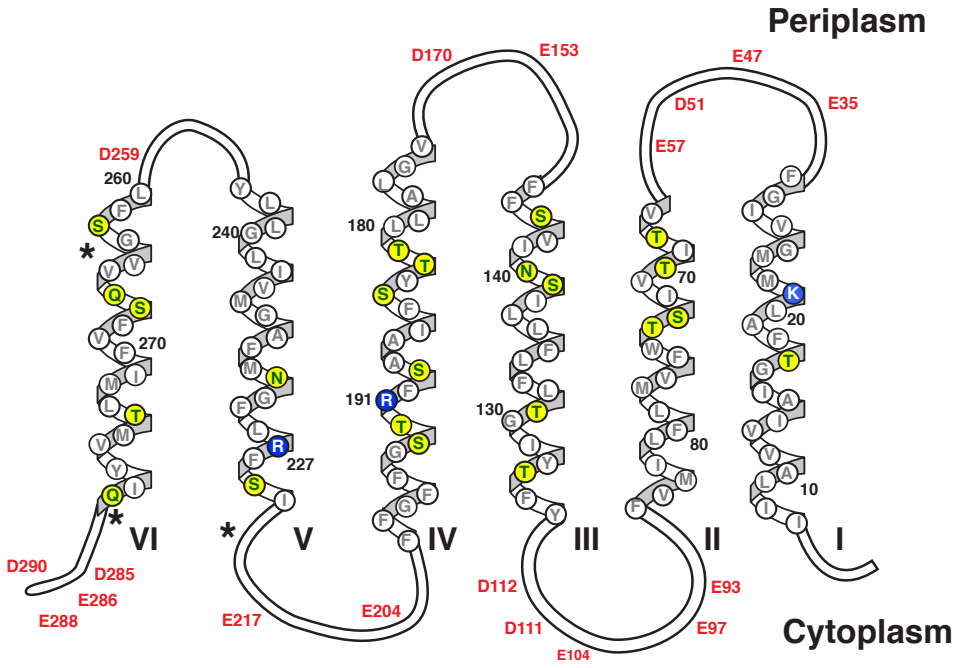

Fig. 9. Amino acid sequence of the a-subunit showing the acidic, basic, and polar residues. The essential stator charge (R227) is on helix V.

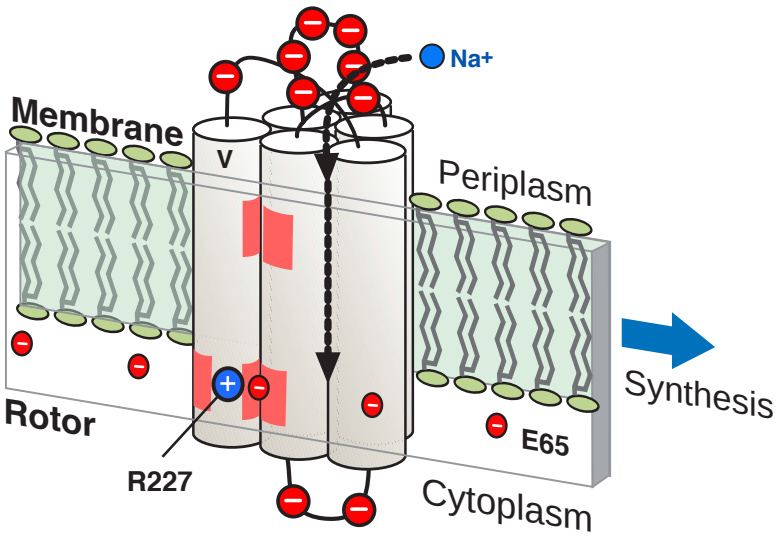

Fig. 10. Detail of the rotor-stator assembly model as viewed from inside the rotor, showing the location of the essential rotor and stator charges and the path of the sodium ion into the stator helix bundle. The ion channel terminates before penetrating all the way through the stator. Red patches indicate polar hydrophilic regions.

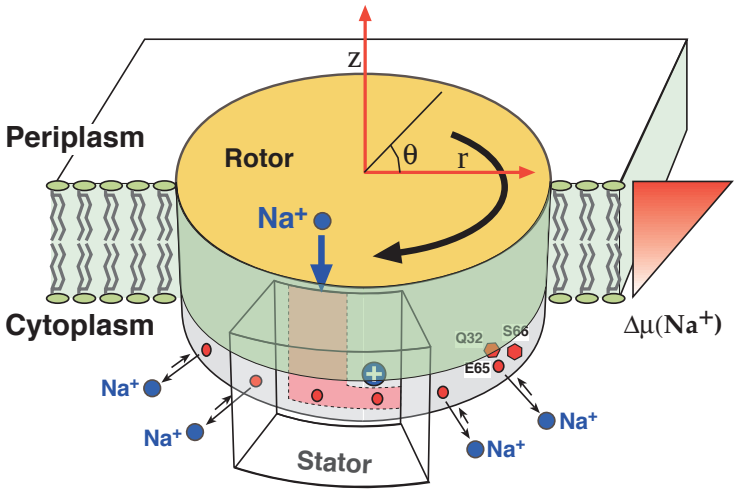

Fig. 11. Schematic of the rotor-stator assembly in *P. modestum* as viewed from outside the rotor. To formulate the mathematical model, a cylindrical coordinate system is established as shown. During ATP synthesis, the rotor turns to the left (clockwise viewed from the periplasm). The rotor section below the level of the membrane contains the 12 ion-binding sites. Each site consists of the triad Q32/E65/S66, which coordinates a sodium ion. Mutation of the ion-binding triad switched the coupling ion from sodium to lithium to protons (1). This strongly suggests that the association between the ions and the rotor sites is strictly electrostatic and can be modeled as a simple Coulomb well as we have done here.

Markov Chain Model for the Evolution of the Rotor State

The ionization state of the rotor-stator assembly is specified by the ionization states of the rotor sites, each of which may be ionized or empty. Because the rotor has 12 ionizable sites, the general chemical state of the rotor can take $2^{12} = 4096$ different values. However, rotor sites far away from the rotor-stator interface do not affect the rotor-stator interaction. Only the 4 rotor sites near the rotor-stator interface interact with the stator, and so specifying their state is sufficient to describe the rotor-stator interaction. Therefore, we define the chemical state of the rotor-stator assembly, denoted by **s**, as the ionization state of the four rotor sites near the rotor-stator interface. Thus there are $2^4 = 16$ possible chemical states.

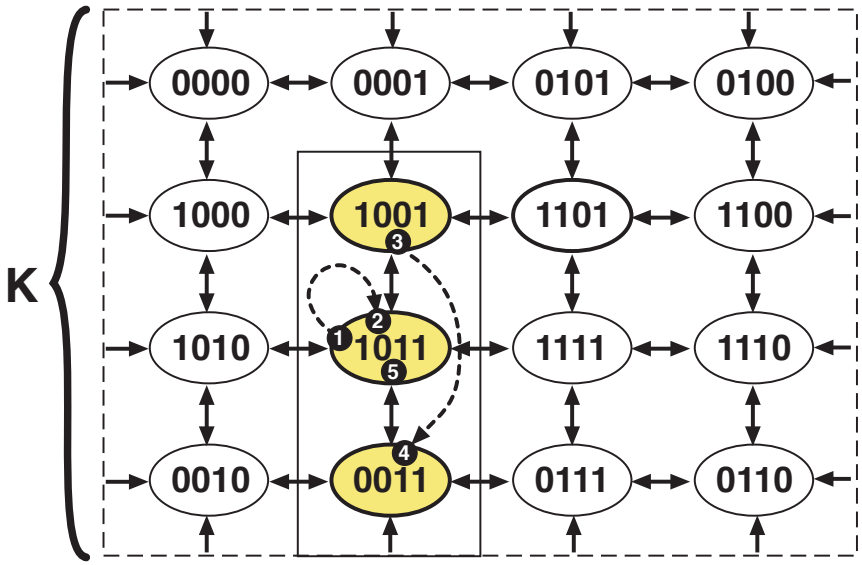

Fig. 12. The Markov transition between the $2^4 = 16$ rotor chemical states can be drawn on a two-dimensional torus. The 16 chemical states are numbered using a binary system as (0000), (0001), … and (1111), where we denote an empty (charged) site by 1 and an occupied (neutral) site by 0. The top of the dashed rectangle is identified with the bottom and the left side with the right. Thus a transition exiting from, say, state (0100) to the right enters state (0000) from the left; if the same state exits upwards, it enters state (0110) from the bottom. Rotations are indicated by dashed lines. The numbers correspond to the sequence of events shown in Fig. 3.

The 16 states can be organized on the surface of a torus; this is shown schematically in Fig. 12. For the convenience of mathematical discussion below, we rename the 16 chemical states as state 1 through state 16. The sequence number, N, of the state $(i_1\ i_2\ i_3\ i_4)$ is given by

$$N = i_1 \times 8 + i_2 \times 4 + i_3 \times 2 + i_4 + 1 \qquad [1]$$

Transitions between states occur when a site binds or releases a sodium ion. Since the relaxation to equilibrium after a proton association/dissociation event is much faster than the mechanical motion of the rotor, we can treat the transitions between these states as a Markov chain (2). Because of the electrostatic interactions between the rotor sites and the stator charge, the transitions between states depend on the angular position of the rotor, denoted θ.

Let $\rho(t, \theta; k)$ be the probability at time t that the system is in the kth state while the angular position of the rotor is fixed at θ. Note that $\rho(t, \theta; k)$ is *not* the probability density at time t that the rotor is at the angular position θ and the system is in the kth state; here θ is a parameter. By fixing the angular position of the rotor, we are able to isolate the kinetics and study its governing equation. In the subsequent sections, we will combine the kinetics and the dynamics to build a complete model for the sodium F_O motor.

The governing equation for the evolution of $\rho(t, \theta; k)$ is

$$\frac{d}{dt}\begin{bmatrix} \rho(t,\theta;1) \\ \rho(t,\theta;2) \\ \vdots \\ \rho(t,\theta;15) \\ \rho(t,\theta;16) \end{bmatrix} = \mathbf{K}(\theta)\cdot \left.\begin{bmatrix} \rho(t,\theta;1) \\ \rho(t,\theta;2) \\ \vdots \\ \rho(t,\theta;15) \\ \rho(t,\theta;16) \end{bmatrix}\right\} 16\,\text{components} \qquad [2]$$

where the transition matrix $\mathbf{K}(\theta)$ is a 16×16 matrix given by

$$\mathbf{K}(\theta) = \begin{bmatrix} -\Sigma_1 & k_{2,1}(\theta) & \cdots & k_{15,1}(\theta) & k_{16,1}(\theta) \\ k_{1,2}(\theta) & -\Sigma_2 & \cdots & k_{15,2}(\theta) & k_{16,2}(\theta) \\ \vdots & \vdots & \ddots & \vdots & \vdots \\ k_{1,15}(\theta) & k_{2,15}(\theta) & \cdots & -\Sigma_{15} & k_{16,15}(\theta) \\ k_{1,16}(\theta) & k_{2,16}(\theta) & \cdots & k_{15,16}(\theta) & -\Sigma_{16} \end{bmatrix} \qquad [3]$$

In the transition matrix $\mathbf{K}(\theta)$, $k_{i,j}(\theta)$ is the transition rate from the ith state to the jth state; the diagonal entry Σ_i is given by

$$\Sigma_i = \sum_j k_{i,j}(\theta) \qquad [4]$$

The transition rate $k_{i,j}(\theta)$ is nonzero only when the ith state and the jth state can be connected by the single event of a sodium ion binding onto or dissociating from a rotor site. For example, the first row of the transition matrix $\mathbf{K}(\theta)$ has four nonzero off-diagonal elements:

- $k_{2,1}(\theta)$: transition rate from state 2 = (0 0 0 1) to state 1 = (0 0 0 0).
- $k_{3,1}(\theta)$: transition rate from state 3 = (0 0 1 0) to state 1 = (0 0 0 0).
- $k_{5,1}(\theta)$: transition rate from state 5 = (0 1 0 0) to state 1 = (0 0 0 0).
- $k_{9,1}(\theta)$: transition rate from state 9 = (1 0 0 0) to state 1 = (0 0 0 0).

The Interaction Between the Rotor and the Stator

To describe the geometry of the rotor-stator assembly, and to calculate the electrostatic interaction between the rotor and stator, we first establish a cylindrical coordinate system as shown in Fig. 11. The z-axis goes through the center of the rotor and is perpendicular to the plane formed by 12 binding sites. The circle of rotor binding sites is defined as $z = 0$. (r, θ) measures the radial distance from the z-axis and the angular distance to a reference line. Fig. 13 shows the rotor stator assembly projected onto θ-z plane and viewed from outside the rotor. The radius of the rotor is taken as 3 nm. Thus the circle of the rotor binding sites has coordinates:

$$r_{\text{site}} = 3.0\,\text{nm}\,; \quad z_{\text{site}} = 0.0\,\text{nm} \qquad [5]$$

We use the angular distance between two adjacent rotor binding sites as a unit displacement, denoted by $\Delta\theta = 2\pi/12$. The four parameters describing the geometry of the rotor-stator assembly in Fig. 13 are

$$\begin{aligned} \theta_1 &= -1.14 \times \Delta\theta \\ \theta_2 &= -0.84 \times \Delta\theta \\ \theta_3 &= 0.5 \times \Delta\theta \\ \theta_4 &= 1.0 \times \Delta\theta \end{aligned} \qquad [6]$$

The positive stator charge, R277, is offset from the circle of rotor binding sites by 0.6 nm in the r direction. It has the coordinates

$$\theta_{\text{R227}} = 0.75 \times \Delta\theta\,; \quad r_{\text{R227}} = 3.6\ \text{nm}\,; \quad z_{\text{R227}} = 0.0\ \text{nm} \qquad [7]$$

A sodium ion bound on a rotor site is offset from that site by 0.3 nm in the r direction. It has the coordinates

$$r_{\text{ion}} = 3.3\ \text{nm}\,; \quad z_{\text{ion}} = 0.0\ \text{nm} \qquad [8]$$

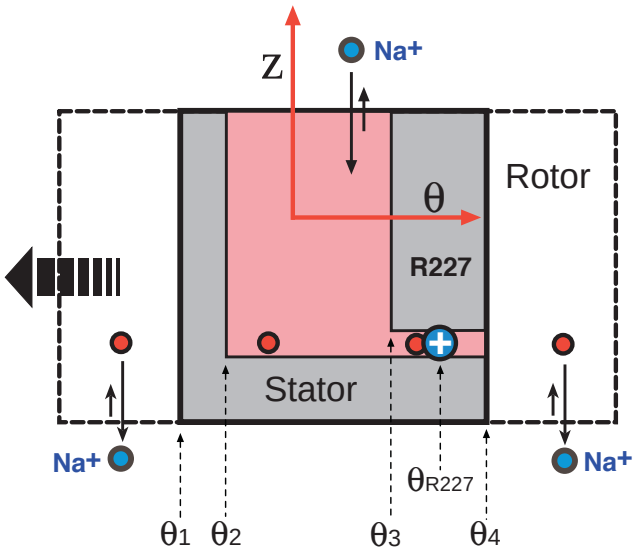

Fig. 13. The rotor-stator assembly projected onto the rotor surface, viewed from outside the rotor. Rotation during synthesis is to the left. If the stator spans three α-helices, then there are four rotor sites located near the stator: two within the rotor-stator interface and two adjacent laterally.

The electrostatic interaction between a charge (a negatively charged rotor binding site or a positively charged sodium ion) and the positive stator charge R227 is calculated using a shielded Coulomb's law. First the interaction according to Coulomb's law is calculated:

$$d(\theta, r, z) = \sqrt{\left[r_{R227}\cos(\theta_{R227}) - r\cos(\theta)\right]^2 + \left[r_{R227}\sin(\theta_{R227}) - r\sin(\theta)\right]^2 + z^2}$$
$$\tilde{\phi}(\theta, r, z) = \frac{e^2}{4\pi\varepsilon_0}\cdot\frac{q}{\varepsilon_S d}\cdot\exp(-\lambda d) = 56\,k_B T\times\frac{q}{\varepsilon d}\cdot\exp(-\lambda d) \qquad [9]$$

In Eq. **9**, (θ, r, z) is the cylindrical coordinate of the charge; $d(\theta, r, z)$ is the distance from the charge to the stator charge R227; q is the valence of the charge: $q = +1$ if the charge is positive (sodium ion) and $q = -1$ if the charge is negative (rotor binding site); ε_S is the dielectric constant of the stator; $1/\lambda$ is the Debye screening length. In our model, we take $\varepsilon_S = 4$ and $1/\lambda = 1$ nm. However, when the charge is in the channel or outside the stator, it is surrounded by an aqueous environment with dielectric constant: $\varepsilon_C \approx 80$. Once outside the stator, the interaction between the charge and R227 is much weaker. Thus we compute the interaction potential between the charge and R227 by modifying the Coulomb's law potential by:

$$\phi(\theta, r, z) = \begin{cases} \tilde{\phi}(\theta, r, z) - \tilde{\phi}(\theta_4, r, z) & \text{if } \theta_3 \le \theta \le \theta_4 \\ 0 & \text{otherwise} \end{cases} \qquad [10]$$

The total electrostatic potential seen by the rotor has three parts:

(*i*) $\phi_Q(\theta, \mathbf{s})$ = the electrostatic interaction between all charges on the rotor and the positive stator charge R227.

(*ii*) $\phi_{\Delta\psi}(\theta, \mathbf{s})$ = the interaction caused by the membrane potential drop.

(*iii*) $\phi_{\Delta\varepsilon}(\theta, \mathbf{s})$ = the interaction caused by the dielectric barrier that opposes the entry of a charged site into the hydrophobic rotor-stator interface.

$\phi_Q(\theta, \mathbf{s})$, is calculated by summing the contributions from the four rotor binding sites near the rotor-stator interface and the contributions from the sodium ions bound on them (if any).

At the level of the rotor binding sites, the potential due to the transmembrane potential drop is given by

$$\phi(\theta) = \begin{cases} \Delta\psi_{\text{mem}} \cdot (\theta - \theta_1) / (\theta_2 - \theta_1) & \text{if } \theta_1 \le \theta \le \theta_2 \\ \Delta\psi_{\text{mem}} & \text{if } \theta_2 \le \theta \le \theta_3 \\ \Delta\psi_{\text{mem}} \cdot (\theta_4 - \theta) / (\theta_4 - \theta_3) & \text{if } \theta_3 \le \theta \le \theta_4 \\ 0 & \text{otherwise} \end{cases} \qquad [11]$$

$\phi_{\Delta\psi}(\theta, \mathbf{s})$ is calculated by summing the contributions from the charged (empty) rotor sites near the rotor-stator interface.

As shown in Fig. 13, the left boundary of the aqueous channel is formed by a rotor-stator interface with low dielectric constant. The effect on an uncharged (occupied) rotor site caused by this dielectric barrier is small; here we take it as zero. However, this dielectric barrier prevents a charged (empty) rotor site from entering the rotor-stator interface. The height of this barrier is given approximately by

$$\Delta\phi = 200\, k_B T \times \left(\frac{1}{\varepsilon_S} - \frac{1}{\varepsilon_C} \right) \approx 45\, k_B T \qquad [12]$$

ε_C and ε_S are the dielectric constants of the cytoplasm and the stator, respectively (3). The potential caused by this dielectric barrier on a charged (empty) rotor site is

$$\phi(\theta) = \begin{cases} 45\, k_B T & \text{if } \theta_1 \le \theta \le \theta_2 \\ 0 & \text{otherwise} \end{cases} \qquad [13]$$

The interaction potential caused by the dielectric barrier, $\phi_{\Delta\varepsilon}(\theta, \mathbf{s})$, is calculated by summing up the contributions from the charged (empty) rotor sites near the rotor-stator interface.

Langevin Equation and Fokker-Planck Equation

The motion of the rotor can be described by equating the viscous drag on the rotor to the torques that act on the rotor and the Brownian force modeling the rotor's thermal fluctuations [i.e. the Langevin equation (4)]:

$$\underbrace{\zeta \frac{d\theta}{dt}}_{\substack{\text{Frictional}\\ \text{drag}}} = \underbrace{\tau_Q(\theta, \mathbf{s})}_{\substack{\text{Rotor - stator}\\ \text{charge interaction}}} + \underbrace{\tau_{\Delta\psi}(\theta, \mathbf{s})}_{\substack{\text{Membrane}\\ \text{potential}}} + \underbrace{\tau_{\Delta\varepsilon}(\theta, \mathbf{s})}_{\substack{\text{Dielectric}\\ \text{barrier}}} + \underbrace{\tau_{RS}(\theta)}_{\substack{\text{Rotor - stator}\\ \text{passive interaction}}} - \underbrace{\tau_L(\theta)}_{\substack{\text{Load torque}\\ \text{from } F_1}} + \underbrace{\tau_B(t)}_{\substack{\text{Brownian}\\ \text{torque}}}, \qquad \underbrace{\mathbf{s} = 1,\ldots,16}_{\substack{\text{Chemical}\\ \text{states}}} \tag{14}$$

where

$$\begin{aligned} \tau_Q(\theta, \mathbf{s}) &= -\frac{\partial \phi_Q(\theta, \mathbf{s})}{\partial \theta} \\ \tau_{\Delta\psi}(\theta, \mathbf{s}) &= -\frac{\partial \phi_{\Delta\psi}(\theta, \mathbf{s})}{\partial \theta} \\ \tau_{\Delta\varepsilon}(\theta, \mathbf{s}) &= -\frac{\partial \phi_{\Delta\varepsilon}(\theta, \mathbf{s})}{\partial \theta} \\ \tau_{RS}(\theta) &= -\frac{\partial \phi_{RS}(\theta)}{\partial \theta} \end{aligned} \tag{15}$$

As discussed above, the three electrostatic torques depend on the chemical state of the rotor site, **s**; that is, whether the site is charged (unoccupied) or uncharged (occupied). For each chemical state, **s**, the sum of the first four terms in Eq. **14** can be expressed as the derivative of a potential function:

$$\tau(\theta, \mathbf{s}) = -\frac{\partial}{\partial \theta}\Phi(\theta, \mathbf{s}) \equiv -\frac{\partial}{\partial \theta}\left(\phi_Q + \phi_{\Delta\psi} + \phi_{\Delta\varepsilon} + \phi_{RS}\right) \tag{16}$$

Thus Eq. **14** can be written compactly as

$$\zeta \frac{d\theta}{dt} = -\frac{\partial \Phi(\theta, \mathbf{s})}{\partial \theta} - \tau_L(\theta) + \tau_B(t), \qquad \mathbf{s} = 1,\ldots,16 \tag{17}$$

In Eq. **17**, ζ is the rotational drag coefficient, θ is the angular coordinate, $\Phi(\theta, \mathbf{s})$ is the sum of the interaction potentials between the rotor and the stator, τ_L is the

load torque, and τ_B is the Brownian torque due to thermal fluctuations. **s** represents the binding status of the four rotor sites near the rotor-stator interface. **s** can take any of the $2^4 = 16$ possible states on the chemical torus shown in Fig. 12. The probability of state **s** evolves according to the kinetic equation **2** , which we rewrite in the paper symbolically as

$$\frac{d}{dt}\mathbf{s} = \mathbf{K}(\theta)\cdot\mathbf{s} \qquad [18]$$

To compute the stochastic behavior of the F_o motor (a sequence of the rotor positions corresponding to different times), Eq. **17** must be solved simultaneously with the Markov process governing the kinetic transitions on the rotor binding sites (Eq. **18**).

For the purpose of computing statistical averages of the motion, such as the load-velocity behavior of the motor, one can recast the model as an equivalent convection diffusion (Fokker-Planck) equation governing the evolution of the probability density (4). In the Fokker-Planck formulation corresponding to Eqs. **17** and **18**, the F_o motor is described by a vector function consisting of 16 probability density functions, one for each chemical state. Let $\rho(\theta, t, \underline{k})$ be the probability density that the rotor is at the angular position θ at time t, and the system is in kth state. Define the probability density vector as:

$$\rho(\theta, t) = \left.\begin{bmatrix} \rho(\theta, t, 1) \\ \rho(\theta, t, 2) \\ \vdots \\ \rho(\theta, t, 15) \\ \rho(\theta, t, 16) \end{bmatrix}\right\} 16 \text{ components} \qquad [19]$$

This probability density vector evolves according to the convection diffusion equations

$$\frac{\partial\rho}{\partial t} = \underbrace{\frac{1}{\zeta}\frac{\partial}{\partial\theta}(\Phi'\rho)}_{\substack{\text{Forces between} \\ \text{rotor and stator}}} + \underbrace{\frac{1}{\zeta}\frac{\partial}{\partial\theta}(\tau_L(\theta)\rho)}_{\text{Load torque}} + \underbrace{D\frac{\partial^2\rho}{\partial\theta^2}}_{\substack{\text{Brownian} \\ \text{motion}}} + \underbrace{\mathbf{K}(\theta)\rho}_{\substack{\text{Transitions} \\ \text{between} \\ \text{rotor states}}} \qquad [20]$$

Here $D = k_B T/\zeta$ is the rotor diffusion coefficient. The 16×16 transition matrix $\mathbf{K}(\theta)$ is defined in Eq. 3. The potential matrix $\Phi(\theta)$ is diagonal and is given by

$$\Phi(\theta) = \underbrace{\left\{ \begin{bmatrix} \Phi(\theta,1) & & & & \\ & \Phi(\theta,2) & & & \\ & & \ddots & & \\ & & & \Phi(\theta,15) & \\ & & & & \Phi(\theta,16) \end{bmatrix} \right.}_{16 \text{ columns}} \left. \right\} 16 \text{ rows} \qquad [21]$$

$\Phi(\theta, k)$, the kth diagonal element of $\Phi(\theta)$, is the electrostatic potential describing the interaction between the rotor and the stator corresponding to the kth chemical state.

Solution of the model equations was performed in Matlab by a finite difference scheme described in ref. 5. The code is available from the authors on request.

Simulations of the Sodium Exchange Experiments

In the sodium exchange experiments of Kaim and Dimroth (6), liposomes with *P. modestum* ATPase contained 100 mM NaCl inside. When the liposomes were exposed to a bath of radioactively labeled 2 mM ^{22}NaCl, sodium ions exchanged between the inside and outside of the liposomes. Since the sodium outside was labeled, the exchange could be measured by the $^{22}Na^+$ found inside liposomes as a function of time. From this the initial $^{22}Na^+$ uptake rate was calculated.

To simulate the exchange between the unlabeled sodium ions inside (Na^+) and the labeled sodium ions outside ($^{22}Na^+$), $^{22}Na^+$ and Na^+ have to be treated as different ionic species. Consequently, the binding status of each rotor site has three possibilities. When we have just one kind of ion, a rotor site is either empty or occupied by an ion. Now the status of a rotor site could be empty, occupied by an unlabeled sodium ion (Na^+), or occupied by a labeled sodium ion ($^{22}Na^+$).

Recall that the chemical state of the rotor is determined by the binding status of the four rotor sites near the rotor-stator interface. Thus the chemical state, **s**, of the rotor has $3^4 = 81$ possibilities. The chemical state is numbered using a ternary system as (0 0 0 0), (0 0 0 1), (0 0 0 2), (0 0 1 0), …, (2 2 2 1), and (2 2 2 2), where a rotor site with an unlabeled sodium ion bound is denoted by 0; an empty rotor site is denoted by 1; a rotor site with a labeled sodium ion bound is denoted by 2.

The governing equation for the Markov chain now has 81 components

$$\frac{d}{dt}\begin{bmatrix}\rho(t,\theta;1)\\ \rho(t,\theta;2)\\ \vdots\\ \rho(t,\theta;80)\\ \rho(t,\theta;81)\end{bmatrix} = \mathbf{K}(\theta)\cdot\left.\begin{bmatrix}\rho(t,\theta;1)\\ \rho(t,\theta;2)\\ \vdots\\ \rho(t,\theta;80)\\ \rho(t,\theta;81)\end{bmatrix}\right\} 81\,\text{components} \qquad [22]$$

For each chemical state, the interaction between the rotor and the stator is calculated using the procedures described above. The calculation of this interaction does not depend on whether the bound sodium ion is labeled. The Fokker-Planck equation for the system has the same form as Eq. **20** except that it now has 81 components instead of 16. Treating $^{22}Na^+$ and Na^+ as two kinds of ions enables us to calculate the flux of $^{22}Na^+$ and the flux of Na^+ separately, from which, the initial $^{22}Na^+$ uptake rate is computed.

Simulating the Behavior of the F_o Pump

A torque generated in F_1 from ATP hydrolysis can drive the F_o motor in reverse turning it into an ion pump. To simulate this behavior, we coupled the mathematical equations for the F_o motor in this paper to the mathematical equations for the F_1 motor formulated by Wang and Oster (5) subject to the following constraints:

- The F_o motor and the F_1 motor rotate with the same velocity.
- The load torque on the F_1 motor (i.e., the torque that the F_1 motor is working against) is the same as the driving torque on the F_o motor.

The resulting ion flux could then be computed by solving the coupled system.

References

1. Kaim, G. & Dimroth, P. (1998) *Biochemisty* **37,** 4626-4634.

2. Elston, T., Wang, H. & Oster, G. (1998) *Nature (London)* **391,** 510-514.

3. Israelachvili, J. (1992) *Intermolecular and Surface Forces* (Academic, New York).

4. Risken, H. (1989) *The Fokker-Planck Equation* (Springer, New York).

5. Wang, H. & Oster, G. (1998) *Nature (London)* **396,** 279-282.

6. Kaim, G. & Dimroth, P. (1998) *EMBO J.* **17,** 5887-5895.